This article has been accepted for publication in IEEE Transactions on Control Systems Technology. This is the author's version which has not been fully edited and content may change prior to final publication. Citation information: DOI 10.1109/TCST.2023.3309503

A multi-layer control strategy for the Calais canal

Pablo Segovia, Vicenç Puig and Eric Duviella

***Abstract*—This paper presents the design of a control strategy for the Calais canal, a navigation canal located in a lowland area in northern France that is affected by tides. Moreover, the available actuators are discrete-valued and the hierarchy of operational objectives is time-varying. All these circumstances render water level regulation of the Calais canal a challenging problem. In view of this situation, the design of the overall control architecture is divided into a sequence of structured tasks, which are distributed among layers. The upper layer determines the current operating mode based on the analysis of several environmental and operational aspects. Information regarding the current mode is taken into account at the intermediate layer to select the appropriate optimization-based control problem, which is solved using lexicographic minimization. The optimal control setpoints are determined and sent to the lower layer, where scheduling problems are solved to select low-level control actions from a finite set to minimize the mismatch with respect to the optimal setpoints. Different realistic simulation scenarios are tested to demonstrate the effectiveness of the proposed approach.**

***Index Terms*—Water resources, water management, multi-layer control, model predictive control.**

I. Introduction

INLAND waterways are large-scale systems consisting of man-made canals and artificial rivers, and are mainly used for navigation and transportation. Transition from road and rail toward inland waterway transport is pursued, as it constitutes an environmentally friendly alternative [1]. Thus, appropriate management policies must be devised for navigational watercourses, especially bearing in mind the current climate change context [2], which constrains system operation. Management of these systems is primarily concerned with the allocation of the available water resources to meet the operational objectives, the most important being safe navigation.

Navigational watercourses are characterized by complex dynamics, spatial distribution of their elements and multi-time scales. Suitable control policies are therefore required to ensure satisfactory system performance for such complex systems, especially if misuse of water resources is to be avoided. Model predictive control (MPC) is one of the most popular approaches [3], as it offers a framework in which physical and operational constraints can be dealt with in a natural manner, and multiple operational objectives can be taken into account simultaneously [4]. Broadly speaking, a dynamic process model is used to predict the effect of controlled inputs on the real system such that the optimal performance—with respect to the chosen criteria—is attained [5]. It is interesting to note that irrigation canal control is an application similar to navigational watercourse control in that both are open-channel systems, and thus the same prediction models may be used in both applications. Research on MPC applied to irrigation canals has received notable attention, see for instance [6], [7], [8], [9], [10], [11], [12], [13], [14].

Despite the commonalities between irrigation canals and navigational watercourses, there is a fundamental difference in terms of operational objectives. While irrigation canal control is mainly concerned with delivering water to end users in a reliable and timely manner, control of navigational watercourses aims to ensure safe vessel navigation by keeping the water levels close to a setpoint known as the normal navigation level (NNL), and within predefined safety bounds—the so-called *navigation interval*—using available infrastructure, e.g., gates, weirs, pumps and valves. Water levels are disturbed as a consequence of external phenomena that can be predicted in time (as e.g., tides), a fact that does generally not affect irrigation canal management. Therefore, navigational watercourse control is characterized by distinct features that set this problem apart from irrigation canal control. In addition to tides, there are two other challenging aspects. On the one hand, actuators are often discrete-valued, i.e., only inputs taking values from a finite set may be applied [15], most notably fixed-speed pumps, which are either off or operate at their design flow, and gates, which typically operate at quantized openings with a resolution of several centimeters. On the other hand, the hierarchy of operational objectives is different depending on the navigational period, i.e., allowed (day) and forbidden (night). The effect of tides is considered in [16], [17], [18], [19], [20], while the use of fixed-speed pumps for control is examined in [16], [17], [21], [22], [18], [19]. However, no paper addresses the use of discrete-valued gates or the issue of time-varying hierarchy of objectives.

The focus of this paper is on water level control of the Calais canal. This navigational watercourse is located in the north of France, and is characterized by all the above features, i.e., its level is affected by tidal periods, a discrete-valued sea outlet gate and fixed-speed pumps are the only available actuators, and navigational and non-navigational periods require to consider a time-varying hierarchy of operational objectives. To the best knowledge of the authors, there is no paper that deals with all these features simultaneously, and thus a new control approach must be developed to ensure satisfactory management of the Calais canal. However, a

This work was supported in part by the Researchlab Autonomous Shipping (RAS) of Delft University of Technology and in part by the Spanish State Research Agency (AEI) and the European Regional Development Fund (ERFD) through the project SaCoAV (ref. MINECO PID2020-114244RB-I00). *(Corresponding author: Pablo Segovia.)*

Pablo Segovia is with the Department of Maritime and Transport Technology, Delft University of Technology, Delft, the Netherlands (e-mail: p.segoviacastillo@tudelft.nl).

Vicenç Puig is with the Research Center for Supervision, Safety and Automatic Control (CS2AC), Universitat Politècnica de Catalunya (UPC), Terrassa, Spain, and also with Institut de Robòtica i Informàtica Industrial (CSIC-UPC), Barcelona, Spain (e-mail: vicenc.puig@upc.edu).

Eric Duviella is with CERI Digital Systems, IMT Nord Europe, Univ. Lille, Lille, France (e-mail: eric.duviella@imt-nord-europe.fr).

monolithic solution is impractical, as this would require to integrate all features in a single model and solve the overall control problem considering a centralized decision mechanism. A common approach to mitigate the inherent modeling and control complexity consists in decomposing the problem into a structured sequence of well-defined and simpler subtasks, each taken care of in a different layer, thus making the problem easier [23]. This approach has been used for systems of different nature, such as nuclear supply systems [24], vehicle platooning applications [25] and hybrid electric vehicles [26].

Summary of the paper and contribution

This paper presents the design of a multi-layer control strategy for water level regulation of the Calais canal. While this paper builds partially on the results presented in [18], [27], [19], the formulation is extended to incorporate some of the issues previously discussed, namely a more in-depth study of environmental and operational aspects, the characterization of the sea outlet gate as a discrete-valued actuator and the consideration of a time-varying hierarchy of objectives. In order to account for all these features, the proposed solution is inspired by the multi-layer paradigm, but the design of each layer and the connection among layers is particular and motivated by the application. Several realistic simulation scenarios are considered in order to test the performance of the approach under different conditions.

Contributions with regard to the current state of the art are:

- Environmental and operational aspects influence system behavior, and are thus analyzed and incorporated into the control design. In particular, the effect of high/low and spring/neap tides is explicitly accounted for, as the Calais canal is directly connected to the sea, and tides have a crucial effect on system performance. Moreover, navigational and non-navigational cycles are distinguished. While this results in an increased number of operating modes, it also provides a more faithful system representation.
- Previous results presented in [18], [27], [19] assumed that the sea outlet gate was able to supply the exact optimal flow setpoints, which is not entirely realistic. This assumption is relaxed in this work, and control actions applied by the gate can only be chosen from a finite set of values, which is moreover time-varying, as it depends on tidal conditions. Furthermore, the time-varying prioritization of operational objectives as a consequence of navigational and non-navigational cycles is also addressed. To the best knowledge of the authors, modeling of gates as discrete actuators and consideration of time-varying hierarchy of objectives in navigational watercourses have not been addressed before.
- The direct application of most cutting-edge research solutions remains infeasible in practice, as the knowledge required is sometimes far from that of the relevant decision makers, i.e., infrastructure managers and operators. Therefore, there exists a gap between state of practice and state of the art in inland waterways management. The proposed approach is inspired by the results presented in [28], [29], [30], [31], where the solutions proposed have led to successful demonstrations on real systems. Aiming to replicate this success, lexicographic minimization [32] is introduced to suit the needs of managers and operators, for whom it is more convenient to define an ordered list of operational objectives arranged by priority, rather than tuning relative priorities using a weighted approach.
- A multi-layer architecture is employed to reduce the complexity of the modelling and control design tasks. Traditional multi-layer approaches for irrigation and navigation canals often determine setpoints at the supervisory level by solving an optimization-based control problem, while the regulatory level often consists in simpler feedback loops using, e.g., PI controllers, in charge of realizing the optimal setpoints. Conversely, the approach presented in this paper solves optimization-based scheduling problems at the lower layer to approximate the optimal setpoint with the available discrete-valued actuators. Such approach has been employed for fixed-speed pumps in [33], [34], [18], [27], [19], but not for discrete-valued gates.
- Finally, although the multi-layer architecture is designed for a particular application, this methodology may be applied to any system that is characterized by several operating modes and discrete-valued actuators.

The rest of the paper is organized as follows. In Section II, a description of the Calais canal is provided. Section III formulates the problem and sketches the main steps to be carried out at each layer. Sections IV–VI describe the upper, intermediate and lower layers, respectively. Section VII summarizes the proposed approach and describes the implementation steps. Section VIII describes the simulation study and discusses the results obtained, allowing to draw conclusions and discuss future research derived from this work in Section IX.

Notation

Let $\mathbb{Z}_{\geq 0}$, $\mathbb{R}^n$ and $\mathbb{R}^{n\times m}$ denote the set of natural non-negative scalars, the space of n-dimensional real column vectors and the space of n-by-m real matrices, respectively. Scalars, vectors and matrices are represented by either lowercase or uppercase letters, bold lowercase letters and bold uppercase letters, respectively, while sets are denoted with calligraphic symbols. All vectors are column vectors unless otherwise stated. Transposition is denoted with $^\intercal$.

II. The Calais canal

Figure 1 presents a schematic representation of the Calais canal, and its physical parameters are summarized in Table I. This canal is located in the Wateringues region in northern France, an area characterized by maritime plains below sea level that are drained using ditches known as watergangs. Excess water is first pumped from the watergangs to the Calais canal, and then released into the sea. To this end, eighteen pumps are installed along the canal so that farmers can empty the watergangs at their convenience.

The Calais canal is a flat navigation canal, and is bounded at the upstream and downstream ends by the lock of Hennuin and the Calais sea outlet gate, respectively. As the canal flows directly into the sea, its management is affected by sea tides.

This article has been accepted for publication in IEEE Transactions on Control Systems Technology. This is the author's version which has not been fully edited and content may change prior to final publication. Citation information: DOI 10.1109/TCST.2023.3309503

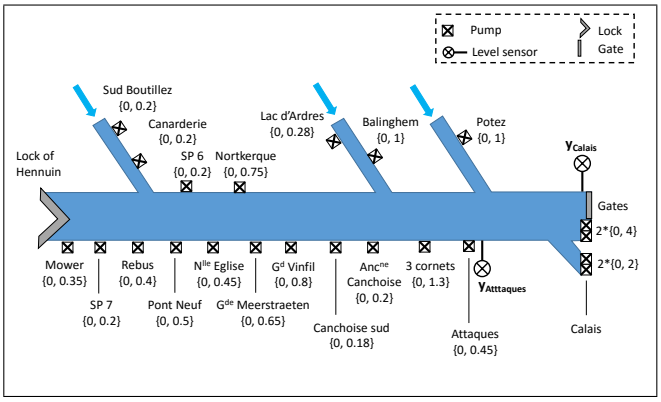

Fig. 1. Simplified view of the Calais canal, adapted from [35]

TABLE I
PHYSICAL PARAMETERS OF THE CALAIS CANAL

Parameter	Value	Parameter	Value	Parameter	Value
LNL [m]	2.05	Length [m]	26720	Bottom slope [m/m]	0
NNL [m]	2.2	Width [m]	20	Manning coeff. [s/m$^{1/3}$]	0.035
HNL [m]	2.35	Side slope [m/m]	0	Average flow [m^3/s]	1

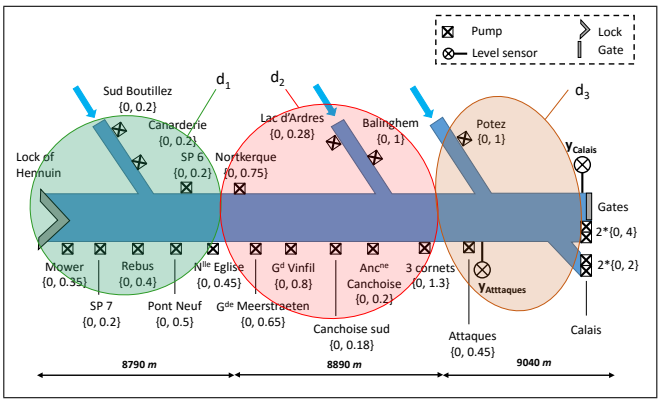

Fig. 2. Simplified view of the Calais canal with disturbance sectors

The Calais canal is also supplied by three secondary canals—currently not regulated—along its water course. As the Calais canal is used for navigation, levels are required to remain within the predefined navigation interval. Therefore, secondary canal inflows, excess water inflows generated by farmers and lock operations at Hennuin have an undesirable impact on the water levels, and are thus regarded as system disturbances. These disturbances are grouped into three disturbance sectors as depicted in Figure 2, following the approach in [35].

As a consequence of the above inflow disturbances, water levels rise, and must be restored to the desired setpoints by releasing water excess into the sea using the available downstream actuators. Therefore, the control strategy must determine the flows that each actuator must supply to track the setpoints and reject the disturbances, using real-time information provided by water level sensors installed in Attaques and Calais. On the one hand, the sea outlet gate can be opened in 0.1 meter intervals. However, the effect of tides is such that the same gate opening leads to different flows through the gate for different tidal conditions (additional details will be provided later on in Section IV). On the other hand, a pumping station consisting of four fixed-speed pumps (two with a design flow equal to 2 m^3/s, and another two with a design flow equal to 4 m^3/s) is also available at the downstream end to release water excess. Operational policies forbid the use of the sea outlet gate during high tide periods to prevent marine water from flowing into the canal. Therefore, water level regulation during high tide periods can only be carried out using pumps.

Several operational goals are expected to be fulfilled during system operation. Below are the most relevant operational objectives identified for the Calais canal:

- Water levels at Attaques and Calais should be kept within the corresponding navigation interval. This objective may be relaxed to account for extreme weather events, which might render the problem temporarily infeasible. In this case, this situation should be penalized to ensure that the water levels are outside the interval as little as possible.
- Water levels at Attaques and Calais should also be kept as close to the normal navigation levels (NNL) as possible. In other words, minimal tracking errors between the water levels and the desired level setpoints should be ensured.
- Economic costs derived from equipment operation should be minimized. Both fixed and variable costs should be considered to account for time-varying electricity prices.
- Control actions applied by the actuators should be as smooth as possible, aiming to extend their useful life.

Although the Calais canal is used for navigation, this is only allowed from 6 a.m. to 8 p.m. Therefore, management of the Calais canal should be carried out in such way that navigation objectives—first and second items of the above list—are prioritized during the corresponding periods. However, these objectives become less important when navigation is forbidden, and less attention may be given at the benefit of reduced operation of the actuators. All in all, management of the Calais canal is driven by navigational and non-navigational cycles, resulting in a time-varying hierarchy of objectives.

III. PROBLEM STATEMENT

The objective of this paper is to determine an appropriate control strategy that is able to fulfill the operational goals for the Calais canal. The control approach should consider the specific features of this system, i.e., the effect of high tides on the use of the sea outlet gate, the existence of discrete-valued actuators and the time-varying hierarchy of objectives. Moreover, the proposed solution should bridge the gap between theory and practice, contributing with a solution that can be of interest to relevant decision makers.

Model-based control approaches are specifically targeted, and therefore a model of the Calais canal is needed. As open-channel flow modeling has been extensively studied, a large number of modeling possibilities are available, among which the integrator delay zero (IDZ) model [36] is selected. This model is obtained from the Saint-Venant nonlinear partial differential equations using simplifying assumptions. Although the Saint-Venant equations provide an accurate representation of the system dynamics, several features, e.g., lack of an analytical solution and sensitivity to geometry inaccuracies, render them unsuitable for real-time control [37]. For a single

This article has been accepted for publication in IEEE Transactions on Control Systems Technology. This is the author's version which has not been fully edited and content may change prior to final publication. Citation information: DOI 10.1109/TCST.2023.3309503

reach—stretch of a canal between two hydraulic structures—this continuous-time input-output model is given by

$$\begin{bmatrix} y^{(1)}(s) \\ y^{(2)}(s) \end{bmatrix} = \begin{bmatrix} p_{11}(s) & p_{12}(s) \\ p_{21}(s) & p_{22}(s) \end{bmatrix} \begin{bmatrix} u^{(1)}(s) \\ u^{(2)}(s) \end{bmatrix}, \tag{1}$$

where $y^{(1)}(s)$ and $y^{(2)}(s)$ denote the upstream and downstream water levels, $u^{(1)}(s)$ and $u^{(2)}(s)$ denote the flows through the upstream and downstream hydraulic structures, and $p_{ij}(s)$ are the IDZ terms, defined as

$$p_{ij}(s) = \frac{z_{ij}s + 1}{A_{ij}s} e^{-\tau_{ij}s}, \tag{2}$$

with $1/A_{ij}$, $-1/z_{ij}$ and τ_{ij} the integrator gain, the zero and the time delay, respectively, for $i, j = \{1, 2\}$. The values of these parameters can be computed for the Calais canal using the data provided in Table I and the formulas given in [36]. Moreover, the following parameters are renamed for convenience: $\{A_{11}, A_{12}\} \triangleq A_u$, $\{A_{21}, A_{22}\} \triangleq A_d$, $\tau_{12} \triangleq \tau_u$ and $\tau_{21} \triangleq \tau_d$. Furthermore, $\tau_{11} = \tau_{22} = 0$.

A discrete-time state-space representation can be obtained from (1) as shown in [38], including disturbances generated at the upstream and downstream ends. This model is given by

$$\begin{aligned} \begin{bmatrix} x^{(1)}_{k+1} \\ x^{(2)}_{k+1} \end{bmatrix} &= \begin{bmatrix} 1 & 0 \\ 0 & 1 \end{bmatrix} \begin{bmatrix} x^{(1)}_{k} \\ x^{(2)}_{k} \end{bmatrix} + \begin{bmatrix} T_s & 0 \\ 0 & -T_s \end{bmatrix} \begin{bmatrix} u^{(1)}_{k} \\ u^{(2)}_{k} \end{bmatrix} \\ &+ \begin{bmatrix} 0 & -T_s \\ T_s & 0 \end{bmatrix} \begin{bmatrix} u^{(1)}_{k-n} \\ u^{(2)}_{k-n} \end{bmatrix} + \begin{bmatrix} T_s & 0 \\ 0 & -T_s \end{bmatrix} \begin{bmatrix} d^{(1)}_{k} \\ d^{(2)}_{k} \end{bmatrix} \\ &+ \begin{bmatrix} 0 & -T_s \\ T_s & 0 \end{bmatrix} \begin{bmatrix} d^{(1)}_{k-n} \\ d^{(2)}_{k-n} \end{bmatrix}, \end{aligned} \tag{3a}$$

$$\begin{aligned} \begin{bmatrix} y^{(1)}_{k} \\ y^{(2)}_{k} \end{bmatrix} &= \begin{bmatrix} \frac{1}{A_u} & 0 \\ 0 & \frac{1}{A_d} \end{bmatrix} \begin{bmatrix} x^{(1)}_{k} \\ x^{(2)}_{k} \end{bmatrix} + \begin{bmatrix} \frac{z_{11}}{A_u} & 0 \\ 0 & -\frac{z_{22}}{A_d} \end{bmatrix} \begin{bmatrix} u^{(1)}_{k} \\ u^{(2)}_{k} \end{bmatrix} \\ &+ \begin{bmatrix} 0 & -\frac{z_{12}}{A_u} \\ \frac{z_{21}}{A_d} & 0 \end{bmatrix} \begin{bmatrix} u^{(1)}_{k-n} \\ u^{(2)}_{k-n} \end{bmatrix} + \begin{bmatrix} \frac{z_{11}}{A_u} & 0 \\ 0 & -\frac{z_{22}}{A_d} \end{bmatrix} \begin{bmatrix} d^{(1)}_{k} \\ d^{(2)}_{k} \end{bmatrix} \\ &+ \begin{bmatrix} 0 & -\frac{z_{12}}{A_u} \\ \frac{z_{21}}{A_d} & 0 \end{bmatrix} \begin{bmatrix} d^{(1)}_{k-n} \\ d^{(2)}_{k-n} \end{bmatrix}, \end{aligned} \tag{3b}$$

where T_s is the sampling time and $n \triangleq \lceil \frac{\max(\tau_u, \tau_d)}{T_s} \rceil$ is the number of delayed samples between the endpoints. It should be noted that navigation canals such as the Calais canal are generally characterized by negligible bottom slopes, and thus $\tau_u \approx \tau_d$. On the other hand, and although the states $\mathbf{x}_k$ have volume units, state-space models obtained from input-output models using canonical forms lead to states without physical interpretation [39]. Moreover, $\mathbf{u}_k$ and $\mathbf{y}_k$ are as defined in (1).

Equation (3) can be particularized for the Calais canal as

$$\begin{aligned} \underbrace{\begin{bmatrix} x^{(A)}_{k+1} \\ x^{(C)}_{k+1} \end{bmatrix}}_{\mathbf{x}_{k+1}} &= \underbrace{\begin{bmatrix} 1 & 0 \\ 0 & 1 \end{bmatrix}}_{\mathbf{A}} \underbrace{\begin{bmatrix} x^{(A)}_{k} \\ x^{(C)}_{k} \end{bmatrix}}_{\mathbf{x}_k} + \underbrace{\begin{bmatrix} 0 \\ -T_s \end{bmatrix}}_{\mathbf{B}_u} \underbrace{\left(u^g_k + \sum_{l=1}^{4} u^{p_l}_k \right)}_{u_k} \\ &+ \underbrace{\begin{bmatrix} -T_s \\ 0 \end{bmatrix}}_{\mathbf{B}_{un}} \underbrace{\left(u^g_{k-n_{A,C}} + \sum_{l=1}^{4} u^{p_l}_{k-n_{A,C}} \right)}_{u_{k-n_{A,C}}} \\ &+ \underbrace{\begin{bmatrix} T_s \\ T_s \end{bmatrix}}_{\mathbf{B}_{dn}} \underbrace{\sum_{i=1}^{3} \sum_{j \in \{A,C\}} d^{(i)}_{k-n_{i,j}}}_{d_{k-n_{i,j}}}, \end{aligned} \tag{4a}$$

$$\begin{aligned} \underbrace{\begin{bmatrix} y^{(A)}_{k} \\ y^{(C)}_{k} \end{bmatrix}}_{\mathbf{y}_k} &= \underbrace{\begin{bmatrix} \frac{1}{A_u} & 0 \\ 0 & \frac{1}{A_d} \end{bmatrix}}_{\mathbf{C}} \underbrace{\begin{bmatrix} x^{(A)}_{k} \\ x^{(C)}_{k} \end{bmatrix}}_{\mathbf{x}_k} + \underbrace{\begin{bmatrix} 0 \\ -\frac{z_{22}}{A_d} \end{bmatrix}}_{\mathbf{D}_u} \underbrace{\left(u^g_k + \sum_{l=1}^{4} u^{p_l}_k \right)}_{u_k} \\ &+ \underbrace{\begin{bmatrix} -\frac{z_{12}}{A_u} \\ 0 \end{bmatrix}}_{\mathbf{D}_{un}} \underbrace{\left(u^g_{k-n_{A,C}} + \sum_{l=1}^{4} u^{p_l}_{k-n_{A,C}} \right)}_{u_{k-n_{A,C}}} \\ &+ \underbrace{\begin{bmatrix} \frac{z_{11}}{A_u} \\ \frac{z_{21}}{A_d} \end{bmatrix}}_{\mathbf{D}_{dn}} \underbrace{\sum_{i=1}^{3} \sum_{j \in \{A,C\}} d^{(i)}_{k-n_{i,j}}}_{d_{k-n_{i,j}}}, \end{aligned} \tag{4b}$$

where $n_{A,C}$ is the number of samples it takes for a control action generated in Calais to have an effect on the water level in Attaques, u^g_k and $u^{p_l}_k$ are the controlled sea outlet gate discharge and the flow supplied by the l-th pump, respectively, $n_{i,j}$ is the number of delayed samples between disturbance origin i (which ranges from one to three to account for the three disturbance sectors introduced in Figure 2) and measurement location j (which is either Attaques or Calais), and $d^{(i)}_{k-n_{i,j}}$ is the delayed effect of disturbance i at location j. Matrices $\mathbf{B}_u$, $\mathbf{B}_{un}$, $\mathbf{D}_u$ and $\mathbf{D}_{un}$ are single-column as there are no upstream actuators in the Calais canal, and thus only the entries corresponding to the downstream actuator are kept. The same holds for $\mathbf{B}_{dn}$ and $\mathbf{D}_{dn}$. However, in the latter case a single disturbance matrix is retained from (3) for each equation. The reason for this is that none of the disturbance origins i are Attaques or Calais, and thus disturbances only have delayed effects at these locations.

An appropriate strategy must be designed to regulate the dynamics of the Calais canal, represented by (4). Following the above discussion on the adequacy of MPC to regulate the water levels, this approach is selected. The optimal input sequences are determined by solving the following open-loop problem:

$$\min_{\left\{u^g_{t|k}\right\}_{t=k}^{k+H_p-1}, \left\{\left\{u^{p_l}_{t|k}\right\}_{t=k}^{k+H_p-1}\right\}_{l=1}^{4}} J\left(u^g_{t|k}, u^{p_l}_{t|k}\right) \tag{5a}$$

subject to

$$\begin{aligned} \mathbf{x}_{t+1|k} &= \mathbf{A}\mathbf{x}_{t|k} + \mathbf{B}_u u_{t|k} + \mathbf{B}_{un} u_{t-n_{A,C}|k} \\ &+ \mathbf{B}_{dn} d_{t-n_{i,j}|k},\ t \in \{k, ..., k+H_p-1\}, \end{aligned} \tag{5b}$$

$$\begin{aligned} \mathbf{y}_{t|k} &= \mathbf{C}\mathbf{x}_{t|k} + \mathbf{D}_u u_{t|k} + \mathbf{D}_{un} u_{t-n_{A,C}|k} \\ &+ \mathbf{D}_{dn} d_{t-n_{i,j}|k},\ t \in \{k, ..., k+H_p-1\}, \end{aligned} \tag{5c}$$

$$u_{t|k} \in \mathcal{U},\ t \in \{k, ..., k+H_p-1\}, \tag{5d}$$

$$\mathbf{x}_{s|k} \in \mathcal{X},\ s \in \{k, ..., k+H_p\}, \tag{5e}$$

$$\mathbf{y}_{t|k} \in \mathcal{Y},\ t \in \{k, ..., k+H_p-1\}, \tag{5f}$$

$$\mathbf{x}_{k+H_p|k} \in \mathcal{X}_{H_p}, \tag{5g}$$

$$\mathbf{x}_{k|k} = \mathbf{x}_k, \tag{5h}$$

with $\{u^g_{t|k}\}_{t=k}^{k+H_p-1} \triangleq \{u^g_{k|k}, u^g_{k+1|k}, \cdots, u^g_{k+H_p-1|k}\}$ and $\{u^{p_l}_{t|k}\}_{t=k}^{k+H_p-1} \triangleq \{u^{p_l}_{k|k}, u^{p_l}_{k+1|k}, \cdots, u^{p_l}_{k+H_p-1|k}\}$, $l = 1, ..., 4$. Moreover, k, t and $k+t|k$ represent the current time instant, the time instant along the prediction horizon, and the predicted value of the variable at instant $k+t$ using information available at instant k, respectively. On the other hand, the cost function $J\left(u_{t|k}\right)$ allows to determine the cost throughout the prediction horizon H_p. Furthermore, $\mathcal{U}$, $\mathcal{X}$ and $\mathcal{Y}$ denote the feasible sets, which are defined according to physical and operational constraints, $\mathcal{X}_{H_p}$ is the terminal constraint set [40], and $\mathbf{x}_k$ is the initial state and can be determined using measurement information. Note that gate and pump actions are explicitly stated as minimization arguments in (5a), while the compact notation introduced in (4) is used in (5b)–(5d) to ease the notation.

The optimal sequences of inputs are then given by $\{u^g_{t|k}\}_{t=k}^{k+H_p-1}$ and $\{u^{p_l}_{t|k}\}_{t=k}^{k+H_p-1}$, $l = 1, ..., 4$. Nevertheless, only $u^g_{k|k}$ and $u^{p_l}_{k|k}$ are retained, according to the receding philosophy $u_k^{MPC(g)} \triangleq u^g_{k|k}$ and $u_k^{MPC(p_l)} \triangleq u^{p_l}_{k|k}$. The problem is solved again at the next time instant to exploit the most recent information, hence converting the original open-loop approach into a closed-loop one.

As stated in Section II, the Calais canal is characterized by multiple environmental and operational aspects with time-varying priority, a fact that requires to define different operating modes. Likewise, the low-level control problem makes the control design more challenging, as (5) is not sufficient to determine the appropriate scheduling of the discrete actuators. Furthermore, the large number of binary variables involved in an MPC formulated for the discrete-valued actuators renders the problem prohibitive to be solved in real time. Therefore, embedding all these phenomena into (4) and solving the overall control problem by designing a single controller based on (5) does not seem to be the most reasonable approach. Instead, resorting to a multi-layer architecture appears to be more convenient.

In view of the above, a three-layer control architecture is proposed to tackle the problem in a structured manner:

- The *upper layer* addresses the characterization of the different operating modes of the Calais canal. These modes are a consequence of time-varying environmental phenomena (high/low and spring/neap tides) and operational conditions (navigational and non-navigational cycles). Aside from characterizing the operating modes, this layer identifies the current mode at every time instant.
- The *intermediate layer* is fed the current operating mode, and adjusts the corresponding settings accordingly. Moreover, the different MPC (one per mode) are designed and solved at this layer using the lexicographic minimization approach. An observer that provides the MPC with the vector of states and information about the disturbances is also designed. The output of this layer is an optimal control setpoint per actuator.
- The *lower layer* receives the optimal control setpoints, and determines the optimal scheduling of the actuators, i.e., which and when these should be activated, such that the combined actions best approximate the setpoints. These actions are applied to the system and their effect is measured, allowing to apply the multi-layer control strategy at the next time instant.

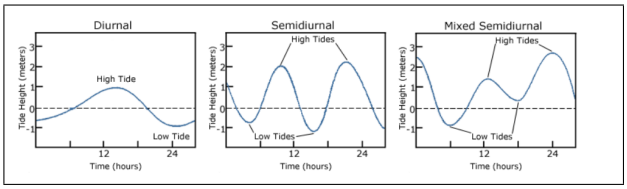

Fig. 3. Types of tidal periods (adapted from [42])

Detailed explanations about the tasks carried out in the upper, intermediate and lower layers are provided in Sections IV, V and VI, respectively.

IV. Upper layer

System operation does not always occur under the same circumstances, a fact that needs to be accounted for at the control design stage to ensure a satisfactory performance. Some of the most relevant environmental and operational phenomena that affect the behavior of open-flow channel systems connected to the sea are described next.

A. Tides

Tides can be defined as the rise and fall of the water levels of the oceans, and are a consequence of gravitational forces exerted by the Sun and the Moon on the Earth. The two main features that characterize tides are the period and the range, and are described following the exposition in [41]. Although tidal responses are rather complex, the elucidations provided below shall suffice for the problem considered in this work.

1) Period: Tidal period can be defined as the time between two consecutive high (low) levels. These can be categorized into three main classes, which are depicted in Figure 3. It is worth noting that each region exhibits a different tidal period depending on its location.

- *Diurnal* tides are characterized by one high and one low tide per day, each with a duration of about twelve hours.
- *Semidiurnal* tides consist of two high and two low tides per day, each with an average duration of six hours. Moreover, the heights of the two high (low) tides are approximately the same.
- *Mixed semidiurnal* tides also exhibit two high and two low tides per day, each lasting about six hours. However, the two high (low) tides differ in height.

The Calais canal can be assumed to exhibit a semidiurnal tidal period, given its location. The main motivation for the consideration of the tidal period stems from the fact that the Calais sea outlet gate cannot be operated in high tide. Therefore, different controllers must be executed during different tidal periods.

This article has been accepted for publication in IEEE Transactions on Control Systems Technology. This is the author's version which has not been fully edited and content may change prior to final publication. Citation information: DOI 10.1109/TCST.2023.3309503

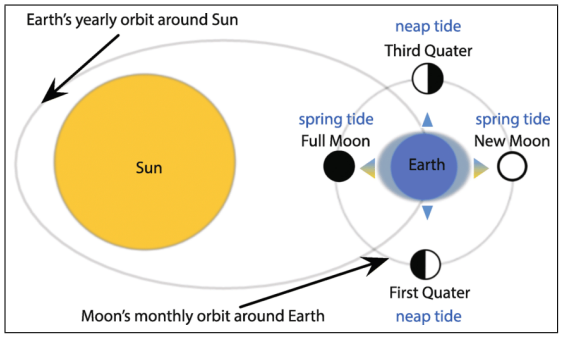

Fig. 4. Tidal ranges: connection with Earth, Sun and Moon relative positions (taken from [43])

TABLE II
CALAIS CANAL SEA OUTLET GATE: OPENINGS AND TIDAL RANGE FLOWS

Opening (m)	Tidal range flow (m^3/s)			Opening (m)	Tidal range flow (m^3/s)		
	Spring	Intermediate	Neap		Spring	Intermediate	Neap
0	0	0	0	1.3	12.7	11.5	10.3
0.1	1.9	1.7	1.4	1.4	13.2	11.9	10.6
0.2	2.7	2.4	2.2	1.5	13.9	12.5	11.1
0.3	4.2	3.8	3.4	1.6	14.0	12.7	11.3
0.4	5.2	4.8	4.3	1.7	14.3	12.9	11.5
0.5	6.6	6	5.4	1.8	14.5	13.1	11.7
0.6	7.6	7	6.3	1.9	14.6	13.3	11.9
0.7	8.6	7.8	7	2	14.7	13.4	12
0.8	9.4	8.7	7.9	2.1	14.8	13.5	12.1
0.9	10.3	9.5	8.5	2.2	14.9	13.6	12.2
1	11.1	10	8.9	2.3	15	13.7	12.3
1.1	11.6	10.5	9.4	2.4	15.1	13.8	12.4
1.2	12.3	11.1	9.8	2.5	15.2	13.9	12.5

2) Range: Tidal range can be defined as the height difference between two consecutive high (low) and low (high) water levels. Two different situations can be distinguished:

- *Spring* tides occur when the Sun, Moon and Earth are aligned, and thus the solar tide has an additive effect on the lunar tide. This phenomenon causes the high (low) tides to be higher (lower) than usual.
- *Neap* tides occur approximately one week later than the spring tides, when the Sun and Moon are at right angles to one another. Then, the solar tide partially cancels out the lunar tide, which results in moderate tides.

The occurrence of the two main tidal ranges is depicted in Figure 4. Each lunar month is characterized by two spring and two neap tides, each with an approximate duration of a week. Needless to say, the transition between the two tidal ranges is not immediate, which motivates the consideration of an *intermediate* tidal range (characterized by average values).

Tidal ranges affect the control design in that the flows delivered by the sea outlet gate are different. More precisely, the same gate opening (in meters) yields different flows (in cubic meters per second) for different tidal ranges, a fact that must be accounted for during the control design. Table II summarizes the admissible sea outlet openings and the corresponding flows during spring, intermediate and neap tidal ranges.

B. Navigational and non-navigational cycles

Navigation, unlike tides, is not an environmental but an operational aspect. Navigational and non-navigational periods are, as the names suggest, characterized by vessels being granted and denied permission to sail, respectively. Common management guidelines dictate that navigation is allowed from morning to evening, and then forbidden until the next morning.

The interest in incorporating this feature lies in the fact that management policies are different for each of the two periods. Although the definition of operational objectives is tackled in the next section, it can be anticipated that greater (lesser) efforts shall be dedicated to guaranteeing safe navigation—as defined in Section I—during navigational (non-navigational) periods. This difference should also be taken into account when designing the controllers.

V. INTERMEDIATE LAYER

The current operating mode is determined at the upper layer. It should be noted that twelve different operating modes can be distinguished, arising from the combination of tidal period (high and low tides), tidal range (spring, intermediate and neap tides), and navigational and non-navigational cycles. This information must be provided to the intermediate layer, so that the appropriate MPC can be solved at each time instant. This issue is tackled in Section V-A. Moreover, MPC requires knowledge of the state vector at the current time instant to generate the optimal input sequence. As discussed in Section III, the states of model (4) are artificial and hence cannot be measured, thus requiring the use of an observer. A moving horizon estimator (MHE) is designed in Section V-B.

A. Control design

The control design starts with the definition and mathematical formulation of operational objectives. The resulting multi-objective optimization problem can then be reformulated to replace the weight selection process with a prioritized list of objectives, an approach that is deemed to be much more in line with the needs of decision makers. Finally, a baseline MPC is designed based on (5), along with the modifications that must be introduced to adapt the baseline MPC to each operating mode.

1) Operational objectives: The operational goals introduced in Section II are listed again for convenience and formulated mathematically:

- Limit amount of time water levels are outside the navigation interval by penalizing the slack variable $\boldsymbol{\alpha}_k$:
$$J_k^{(1)} = \boldsymbol{\alpha}_k^\intercal \boldsymbol{\alpha}_k. \tag{6}$$
- Keep water levels as close to the NNL as possible:
$$J_k^{(2)} = (\mathbf{y}_k - \mathbf{y}_{NNL})^\intercal (\mathbf{y}_k - \mathbf{y}_{NNL}), \tag{7}$$
with $\mathbf{y}_{NNL}$ the vector of NNL values.
- Minimize costs derived from equipment operation:
$$J_k^{(3)} = \left(\beta^{(1)} + \beta_k^{(2)}\right) u_k, \tag{8}$$
with $\beta^{(1)}$ and $\beta_k^{(2)}$ the fixed and variable electricity costs, respectively. Note that u_k denotes both sea outlet gate and pumping actions, as defined in (4).
- Ensure smoothness of control actions:
$$J_k^{(4)} = (\Delta u_k)^2, \tag{9}$$
with $\Delta u_k = u_k - u_{k-1}$.

This article has been accepted for publication in IEEE Transactions on Control Systems Technology. This is the author's version which has not been fully edited and content may change prior to final publication. Citation information: DOI 10.1109/TCST.2023.3309503

2) Lexicographic minimization: Consideration of the operational objectives introduced in Section V-A1 results in a multi-objective optimization problem. One of the most common approaches to solve such problems consists in building a scalar cost function as the weighted sum of individual cost functions, wherein the most important objectives are typically assigned larger weights. However, this approach presents two main drawbacks. On the one hand, selecting an appropriate set of weights is not a trivial task [32]. On the other hand, a single set of weights does not guarantee that such objectives are prioritized for all operating conditions [44], thus rendering this approach scenario-dependent.

It is not unusual that two or more objectives of conflicting nature are considered [45], e.g., objectives (7) and (8). Then, the problem consists in selecting the available decision alternative that results in the best compromise [46]. A large amount of methods exist to determine the best compromise alternative. These can be classified into a-priori, interactive and a-posteriori methods, depending on the stage at which the decision maker is involved [47].

- A-priori methods utilize the preference structure defined by the decision maker to convert the multi-objective problem into a single-objective problem. Then, its solution determines the alternative that should be applied.
- Interactive approaches follow the same principles than a-priori methods. However, solution of the problem is used by the decision maker to refine the preference structure. The problem is solved in an iterative manner until a satisfactory solution is found.
- A-posteriori strategies compute a set of efficient alternatives, which are all assumed to have the same preference. The decision maker then analyzes trade-offs and selects among the available alternatives.

A-posteriori methods offer the advantage that searching and decision are tackled independently, which allows for a more informed final decision [47]. The main drawback resides precisely in the fact that the Pareto-optimal solution is not unique. Therefore, it is not straightforward to select among the available alternatives. Conversely, if an initial hierarchy of objectives can be formulated, a unique optimal solution in the Pareto front exists [48]. Such solution is a special type of Pareto-optimal solution that incorporates ordering of objectives, and is known as a *lexicographic solution*. This is the case for the Calais canal, where a clear hierarchy of operational objectives can be determined for each of the twelve operating modes.

Let a set of L operational objectives be ranked according to their priority, where $f_1(\mathbf{z})$ and $f_L(\mathbf{z})$ are scalar functions that denote the most and least important objectives, respectively, and $\mathbf{z} \in \mathcal{Z}$ represents the vector of optimization variables. Then, a solution $\mathbf{z}^*$ is a lexicographic minima if and only if a certain objective can only be improved by deteriorating at least one objective with a higher priority [32]. A standard approach to find a lexicographic solution consists in solving single-objective optimization problems in a sequential manner, considering the most important objective first, and the least important objective last. In order to ensure that the solution of a lower-priority, single-objective optimization problem does not deteriorate performance computed for more important objectives, additional constraints are imposed. This procedure is sketched in Algorithm 1, and can be easily incorporated into the control problem design.

Algorithm 1 Lexicographic multi-objective optimization approach

1: $f_1^* = \min_{\mathbf{z}\in\mathcal{Z}} f_1(\mathbf{z})$
2: **for** $i = 2 : L$ **do**
3: $\quad f_i^* = \min\left\{f_i(\mathbf{z}) | f_j(\mathbf{z}) \leq f_j^*,\, j = 1, ..., i-1\right\}$
4: **end for**
5: Set lexicographic minimizer as: $\mathbf{z}^* \in \{\mathbf{z} \in \mathcal{Z} | f_i(\mathbf{z}) \leq f_i^*,\, i = 1, ..., L\}$

3) MPC formulation: An MPC based on Eq. (5) is designed to compute the set of optimal references, taking into account the operational objectives (6)–(9). As mentioned before, different operating modes, which result from the combination of the features described in Section IV, characterize system operation at different time instants, each with its own hierarchy of objectives.

With all this, the MPC that is solved for the r-th operational objective can be formulated based on (5) as follows:

$$\min_{\left\{u^g_{t|k}\right\}_{t=k}^{k+H_p-1},\, \left\{\left\{u^{p_l}_{t|k}\right\}_{t=k}^{k+H_p-1}\right\}_{l=1}^{4}} J^{(r)}\left(u^g_{t|k}, u^{p_l}_{t|k}\right) \quad (10a)$$

subject to:

$$\mathbf{x}_{t+1|k} = \mathbf{A}\mathbf{x}_{t|k} + \mathbf{B}_u u_{t|k} + \mathbf{B}_{un} u_{t-n_{A,C}|k} + \mathbf{B}_{dn} d_{t-n_{i,j}|k},\ t \in \{k, ..., k+H_p-1\}, \quad (10b)$$

$$\mathbf{y}_{t|k} = \mathbf{C}\mathbf{x}_{t|k} + \mathbf{D}_u u_{t|k} + \mathbf{D}_{un} u_{t-n_{A,C}|k} + \mathbf{D}_{dn} d_{t-n_{i,j}|k},\ t \in \{k, ..., k+H_p-1\}, \quad (10c)$$

$$\underline{u}^g \leq u^g_{t|k} \leq \overline{u}^g,\ t \in \{k, ..., k+H_p-1\}, \quad (10d)$$

$$\underline{u}^{p_l} \leq u^{p_l}_{t|k} \leq \overline{u}^{p_l},\ t \in \{k, ..., k+H_p-1\},\ l = 1, ..., 4, \quad (10e)$$

$$\underline{\mathbf{y}} - \boldsymbol{\alpha}_{t|k} \leq \mathbf{y}_{t|k} \leq \overline{\mathbf{y}} + \boldsymbol{\alpha}_{t|k},\ t \in \{k, ..., k+H_p-1\}, \quad (10f)$$

$$\boldsymbol{\alpha}_{t|k} \geq \mathbf{0},\ t \in \{k, ..., k+H_p-1\}, \quad (10g)$$

$$\mathbf{x}_{k|k} = \hat{\mathbf{x}}^{MHE}_{k-1}, \quad (10h)$$

$$d_{m|k} = \hat{\mathbf{d}}^{MHE}_m,\ m \in \{k - n_{i,j}, ..., k\}, \quad (10i)$$

$$d_{o|k} = \hat{\mathbf{d}}^{hist}_o,\ o \in \{k+1, ..., k+H_p-n_{i,j}-1\}, \quad (10j)$$

$$u^g_{s|k} = u^{MPC(g)}_s,\ s \in \{k - n_{A,C}, ..., k-1\}, \quad (10k)$$

$$u^{p_l}_{s|k} = u^{MPC(p_l)}_s,\ s \in \{k - n_{A,C}, ..., k-1\},\ l = 1, ..., 4, \quad (10l)$$

$$J^{(q)} \leq J^{(q,*)},\ q = 1, ..., r-1, \quad (10m)$$

where $\boldsymbol{\alpha}_k$ is the slack variable introduced in (6), the single-objective cost function $J^{(r)}$ describes the r-th operational goal and $J^{(q,*)}$ denotes the optimal value determined for the q-th objective during the resolution of the q-th subproblem. Furthermore, (10b) and (10c) constitute the system model

given by (4), (10d) and (10e) set lower and upper bounds on the gate and pumping actions, respectively, (10f) and (10g) denote relaxed upper and lower bounds on the water levels and positiveness of the slack variable, respectively, (10h) and (10i) set the values of the delayed states and disturbances estimated by the MHE in previous iterations, respectively, (10j) uses available historical data for future disturbance values (see Remark 1), (10k) and (10l) set the values of the delayed gate and pumping control actions computed in past MPC iterations, respectively, and (10m) is introduced to solve the single-objective optimization problems following the lexicographic minimization approach sketched in Algorithm 1.

Remark 1. Note that the MHE in Section V-B provides disturbance estimates until the current time instant as reflected in (10i), as it uses past input-output data. For the remaining time instants within the prediction horizon, an estimation based on historical data is used as indicated in (10j). □

Solution of (10) determines the optimal sequences $\{u^g_{t|k}\}^{k+H_p-1}_{t=k}$ and $\{u^{p_l}_{t|k}\}^{k+H_p-1}_{t=k}$, $l = 1, ..., 4$, which are defined as in Section III. Nevertheless, only $u^g_{k|k}$ and $u^{p_l}_{k|k}$ must be fed to the lower layer, following the receding philosophy $u^{MPC(g)}_k \triangleq u^g_{k|k}$ and $u^{MPC(p_l)}_k \triangleq u^{p_l}_{k|k}$.

Equation (10) constitutes the baseline MPC. The following remarks are introduced to account for different operating modes.

Remark 2. As mentioned in Section II, the sea outlet gate cannot be used during high tide to prevent marine water from flowing into the canal. Therefore, (10) represents the low-tide MPC, and the high-tide MPC can be formulated by removing $u^g_{t|k}$ and $u^g_{t-n|k}$ from (10). □

Remark 3. In connection to the previous point, while both gate and pumps can be used during low tide periods, the use of the former is preferred over the latter for economic and operational reasons. This can be addressed by splitting $J^{(3)}_k$ in (8) into $J^{(3,g)}_k$ (gate) and $J^{(3,p)}_k$ (pumps), and $J^{(4)}_k$ in (9) into $J^{(4,g)}_k$ (gate) and $J^{(4,p)}_k$ (pumps). Then, higher priorities can be assigned to $J^{(3,p)}_k$ and $J^{(4,p)}_k$ over $J^{(3,g)}_k$ and $J^{(4,g)}_k$, respectively, as an early optimization of these objectives results in an increasingly constrained pump usage. □

Remark 4. Operating modes characterized by a navigational (non-navigational) cycle rank $J^{(1)}_k$ and $J^{(2)}_k$ higher (lower) in the hierarchy of objectives. □

Remark 5. The different tidal ranges presented in Section IV-A2 are characterized by different gate flows for the same gate opening. Then, $\underline{u}^g$ and $\overline{u}^g$ in (10d) must be adapted for each operating mode, using the values in Table II. □

B. Observer design

State and disturbance estimates are provided to the MPC, thus allowing to determine the optimal gate and pumping actions. On the one hand, the state vector is required to compute the control actions. As these are not directly available for measurement, an observer is needed. This is also true for systems with artificial states, e.g., state-space models obtained from input-output models [39], which is the case of (4). On the other hand, disturbance estimates can be used by the controller to yield optimal control actions whose expected effect matches closely the measured effect on the real system.

Moving horizon estimation (MHE) is employed for state and disturbance estimation, given the similarities shared with MPC. Its main principle consists in using a sliding window of fixed length to process only part of the system inputs and outputs [49]. The estimation problem is formulated as a quadratic program, and a truncated sequence of estimates is determined at each time instant [50]. The moving window is then shifted in time to process only the most recent information, thus keeping the problem bounded in size [51].

Therefore, state and disturbance estimates can be obtained by solving the following MHE:

$$\min_{\substack{\{\hat{\mathbf{x}}_{t|k}\}^{k+1}_{t=k-N+1},\\ \{\hat{d}_{t|k}\}^{k}_{t=k-N+1}}} \mathbf{w}^\intercal_{k-N+1|k}\mathbf{P}^{-1}\mathbf{w}_{k-N+1|k} + \sum_{t=k-N+1}^{k}\left(\mathbf{w}^\intercal_{t|k}\mathbf{Q}^{-1}\mathbf{w}_{t|k} + \mathbf{v}^\intercal_{t|k}\mathbf{R}^{-1}\mathbf{v}_{t|k}\right) \tag{11a}$$

subject to:

$$\mathbf{w}_{k-N+1|k} = \hat{\mathbf{x}}_{k-N+1|k} - \mathbf{x}_{k-N+1}, \tag{11b}$$

$$\begin{aligned}\mathbf{w}_{t|k} = \hat{\mathbf{x}}_{t+1|k} - \big(&\mathbf{A}\mathbf{x}_{t|k} + \mathbf{B}_u u_{t|k} \\ &+\mathbf{B}_{un}u_{t-n_{A,C}|k} + \mathbf{B}_{dn}d_{t-n_{i,j}|k}\big), \\ &t \in \{k-N+1, ..., k\},\end{aligned} \tag{11c}$$

$$\begin{aligned}\mathbf{v}_{t|k} = \mathbf{y}_{t|k} - \big(&\mathbf{C}\mathbf{x}_{t|k} + \mathbf{D}_u u_{t|k} \\ &+\mathbf{D}_{un}u_{t-n_{A,C}|k} + \mathbf{D}_{dn}d_{t-n_{i,j}|k}\big), \\ &t \in \{k-N+1, ..., k\},\end{aligned} \tag{11d}$$

$$\mathbf{y}_{t|k} = \mathbf{y}_t,\ t \in \{k-N+1, ..., k\}, \tag{11e}$$

$$\hat{d}_{t|k} \geq \mathbf{0},\ t \in \{k-N+1, ..., k\}, \tag{11f}$$

$$\underline{\mathbf{x}} \leq \hat{\mathbf{x}}_{s|k} \leq \overline{\mathbf{x}},\ s \in \{k-N+1, ..., k+1\}, \tag{11g}$$

$$\hat{d}_{m|k} = \hat{d}^{MHE}_m,\ m \in \{k-N-n_{i,j}+1, ..., k-N\}, \tag{11h}$$

$$u^g_{o|k} = u^{MPC(g)}_o,\ o \in \{k-N-n_{A,C}+1, ..., k\}, \tag{11i}$$

$$u^{p_l}_{o|k} = u^{MPC(p_l)}_o,\ o \in \{k-N-n_{A,C}+1, ..., k\}, \tag{11j}$$

where $\mathbf{w}_k$ and $\mathbf{v}_k$ denote system disturbances and measurement noise, respectively, N is the estimation window length, $\mathbf{P}^{-1}$, $\mathbf{Q}^{-1}$ and $\mathbf{R}^{-1}$ are weighting matrices inverses of appropriate dimensions, $\mathbf{x}_{k-N+1}$ denotes the most likely initial state, $\mathbf{y}_t$ represents the measured water levels, and the rest of variables and parameters are as in (10). On the other hand, (11) corresponds to the low-tide MHE; the high-tide MHE can be derived by removing $\mathbf{u}^g_{t|k}$ and $\mathbf{u}^g_{t-n|k}$ from (11).

Solution of (11) yields the optimal sequences $\{\hat{\mathbf{x}}_{t|k}\}^{k+1}_{t=k-N+1}$ and $\{\hat{d}_{t|k}\}^{k}_{t=k-N+1}$. Nevertheless, as is the case in the MPC, a single value of each sequence is retained. In the MHE, this corresponds to the last value. Thus, $\hat{\mathbf{x}}^{MHE}_k \triangleq \hat{\mathbf{x}}_{k+1|k}$ and $\hat{d}^{MHE}_k \triangleq \hat{d}_{k|k}$.

This article has been accepted for publication in IEEE Transactions on Control Systems Technology. This is the author's version which has not been fully edited and content may change prior to final publication. Citation information: DOI 10.1109/TCST.2023.3309503

VI. Lower layer

The intermediate layer sends $u_k^{MPC(g)}$ and $u_k^{MPC(p_l)}$, with $l = 1, ..., 4$, to the lower layer, using a sampling time equal to T_{s_1}. This information is used to schedule the operation of the sea outlet gate and the pumps, which work with a sampling time equal to T_{s_2}, with $T_{s_2} < T_{s_1}$. More precisely, the scheduling strategy determines, for each actuator, the sequence of M feasible low-level control actions that minimizes the mismatch with its optimal setpoint, with $M = T_{s_1}/T_{s_2}$. As a result, the low-level control actions to be applied to the system between two consecutive optimal setpoints are determined.

The need for actuator scheduling arises due to the presence of discrete-valued actuators in the Calais canal, which hinders realization of the exact optimal setpoints. However, while the pumps are of fixed-speed nature (ON/OFF), the sea outlet gate can be opened at predefined intermediate positions as noted in Table II. This fact renders the two scheduling problems slightly different.

Gate and pumping scheduling problems are designed below. Their operation is expected to achieve two objectives. First and foremost, the solution of the lower layer should match that of the intermediate layer as closely as possible, in terms of total volumes of water released into the sea. A secondary objective consists in maximizing smoothness of the discrete action, in the same spirit as (9). This fact defines two bi-objective optimization-based scheduling problems. As such, the lexicographic minimization approach introduced in Section V-A2 can be applied.

A. Sea outlet gate scheduling

The gate scheduling problem can be formulated as follows. Let $u_{kM}^{MPC(g)} \triangleq u_k^{MPC(g)}$ denote the optimal sea outlet gate flow determined by the MPC at the k-th time instant, but expressed using the sampling time of the lower layer, with $k \in \mathbb{Z}_{\geq 0}$. Moreover, let u_i^g denote the flow that must be supplied by the gate at the i-th time instant. This value must be chosen from a finite set of values.

The solution of the sea outlet gate scheduling problem is given by the sequence $\mathbf{u}^g \triangleq \{u_t^g\}_{t=kM}^{(k+1)M-1}$, which is determined taking the following two operational objectives into account:

- Minimize mismatch between intermediate and lower layer solutions:

$$J_{kM}^{(g,1)} = T_{s_1} u_{kM}^{MPC(g)} - T_{s_2} \sum_{t=kM}^{(k+1)M-1} u_t^g. \tag{12}$$

- Maximize smoothness of the solution:

$$J_{kM}^{(g,2)} = \sum_{t=kM}^{(k+1)M-1} \left(u_t^g - u_{t-1}^g\right)^2, \tag{13}$$

  and u_{kM-1}^g is the last value of the previous scheduling sequence.

Then, the sea outlet gate scheduling problem can be formulated (for the r-th objective) as follows:

$$\min_{\{u_t^g\}_{t=kM}^{(k+1)M-1}} J_{kM}^{(g,r)} \tag{14a}$$

subject to:

$$u_t^g \in \mathcal{Q}_m^g,\ t \in \{kM, ..., (k+1)M-1\}, \tag{14b}$$

$$u_{t+l_g}^g = u_t^g,\ t \in \{kM, ..., (k+1)M-1-l_g\}, \tag{14c}$$

$$l_g \in \mathbb{Z}_{\geq 0},$$

$$J^{(g,q)} \leq J^{(g,q,*)},\ q = 1, ..., r-1, \tag{14d}$$

where $\mathcal{Q}_m^g$ in (14b) denotes the discrete set of possible flows that the gate can deliver during the m-th operating mode, which are given in Table II. Moreover, (14c) borrows ideas from the unit commitment problem [52] to limit high-frequency switching of the position of the gates. It is assumed that the same flow must be supplied by the gate during at least l_g consecutive low-level sampling instants, where l_g is a design parameter. Furthermore, (14d) follows from the application of the lexicographic minimization approach.

B. Pump scheduling

Formulation of the pump scheduling problem follows the same ideas in Section VI-A, but bearing in mind that pumps are binary actuators. Let $u_{kM}^{MPC(p_l)} \triangleq u_k^{MPC(p_l)}$ denote the optimal action determined by the MPC for the l-th pump at the k-th time instant, but expressed using the sampling time of the lower layer, with $k \in \mathbb{Z}_{\geq 0}$. Moreover, let $s_t^{(l)}$ denote the activation state of the l-th pump at the t-th time instant, $l = 1, ..., 4$, $t = kM, ..., (k+1)M-1$, which equals 1 when the pump is ON and 0 when it is OFF. Moreover, $u_d^{(l)}$ represents the design flow of the l-th pump, $l = 1, ..., 4$.

The solution of the pump scheduling problem is given by the sequences $\mathbf{s}^{(l)} \triangleq \left\{s_t^{(l)}\right\}_{t=kM}^{(k+1)M-1}$, $l = 1, ..., 4$, which are determined considering the same operational objectives:

- Minimize mismatch between intermediate and lower layer solutions:

$$J_{kM}^{(p,1)} = T_{s_1} \sum_{l=1}^{4} u_{kM}^{MPC(p_l)} - T_{s_2} \sum_{t=kM}^{(k+1)M-1} \sum_{l=1}^{4} u_d^{(l)} s_t^{(l)}. \tag{15}$$

- Maximize smoothness of the solution:

$$J_{kM}^{(p,2)} = \sum_{t=kM}^{(k+1)M-1} \sum_{l=1}^{4} \left(s_t^{(l)} - s_{t-1}^{(l)}\right)^2, \tag{16}$$

  and $s_{kM-1}^{(l)}$ is the last value of the previous scheduling sequence for the l-th pump, $l = 1, ..., 4$.

Then, the pump scheduling problem can be formulated (considering the r-th objective) as follows:

$$\min_{\left\{\left\{\mathbf{s}_t^{(l)}\right\}_{t=kM}^{(k+1)M-1}\right\}_{l=1}^{4}} J_{kM}^{(l,r)} \tag{17a}$$

This article has been accepted for publication in IEEE Transactions on Control Systems Technology. This is the author's version which has not been fully edited and content may change prior to final publication. Citation information: DOI 10.1109/TCST.2023.3309503

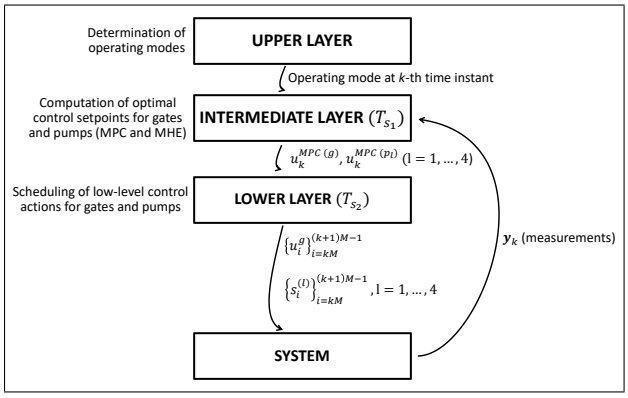

Fig. 5. Multi-layer control architecture, including information exchanges

subject to:

$$s_t^{(l)} \in \{0,1\},\ t = kM, ..., (k+1)M-1,\ l = 1, ..., 4, \tag{17b}$$

$$s_{t+l_p}^{(l)} = s_t^{(l)}, \quad t \in \{kM, ..., (k+1)M-1-l_p\},\ l_p \in \mathbb{Z}_{\geq 0}, \tag{17c}$$

$$J^{(p,q)} \leq J^{(p,q,*)},\ q = 1, ..., r-1, \tag{17d}$$

$$s_t^j(l+1) + \left(1 - s_t^j(l)\right) \leq 1,\ t \in \{kM, ..., (k+1)M-1-l_g\},\ l = 1, ..., 3, \tag{17e}$$

where (17c) ensures that the activation state of each pump is kept constant for at least l_p consecutive low-level sampling instants, (17d) is introduced to solve the pump scheduling problem using the lexicographic minimization approach, and (17e) ensures the sequential activation of the pumps as in [34, Eq. (10)], whereby the l-th pump must be active before the $(l+1)$-th pump can be activated.

VII. Multi-layer approach implementation

Descriptions of the steps carried out in the upper, intermediate and lower layer have been provided in Sections IV, V and VI, respectively, together with dependencies in terms of required information. As mentioned in Section III, tackling the overall problem using a multi-layer control architecture improves computational efficiency. What is more, a centralized, single-layer implementation would suffer from scalability issues given the large number of binary variables, which is due to the discrete-valued nature of the Calais canal actuators.

An overview of the multi-layer architecture is depicted in Figure 5. This figure includes a description of the main task carried out at each layer, as well as their inputs and outputs, and their interaction with the system.

The multi-layer architecture implementation is sketched in Algorithm 2. Its execution is carried out using the fastest sampling time—which is T_{s_2} and corresponds to that of the lower layer. As the intermediate layer runs with a sampling time of T_{s_1}, it must be executed only once every M time instants, according to the current operating mode that is determined at the upper layer. This information is used at the intermediate layer to solve the appropriate MPC once every M time instants, which yields the optimal control setpoints.

Algorithm 2 Multi-layer architecture implementation

Require: parameters in (10), (11), (14), (17)

Estimate $\hat{\mathbf{x}}_0$ and $\hat{\mathbf{d}}_0$ using (11)
Set $\hat{\mathbf{x}}^{MHE} = \hat{\mathbf{x}}_0$ and $\hat{d}^{MHE} = \hat{d}_0$
for $t = 0 : T_{sim}$ **do**
  if $\text{mod}(t, M) = 0$ **then**
    Determine operating mode at instant t (and also at instants within prediction horizon) at upper layer
    Solve the corresponding MPC problems (10) using $\hat{\mathbf{x}}^{MHE}$ and $\hat{d}^{MHE}$
    Extract $u_t^{MPC(g)}$ and $u_t^{MPC(p_l)}$, $l = 1, ..., 4$
    Solve gate scheduling problem (14) using $u_t^{MPC(g)}$ and determine sequence u^g
    Solve pump scheduling problem (17) using $\mathbf{u}_t^{MPC(p_l)}$ and determine sequences $\mathbf{s}^{(l)}$, $l = 1, ..., 4$
  end if
  Apply $(\text{mod}(t, M) + 1)$-th components of $\mathbf{u}^g$ and $\mathbf{s}^{(l)}$, $l = 1, ..., 4$ to the system
  if $\text{mod}(t, M) = M - 1$ **then**
    Measure $\mathbf{y}$
    Solve (11) using the N last values of $\mathbf{y}$, $\text{sum}(\mathbf{u}^g)$ and $\text{sum}\left(\mathbf{u}_d^{(l)}\mathbf{s}^{(l)}\right)$, $l = 1, ..., 4$
    Extract $\hat{\mathbf{x}}^{MHE}$ and $\hat{d}^{MHE}$
  end if
end for

These values are sent to the lower layer, where scheduling problems are solved to determine the sequences of M low-level control actions. These are applied sequentially to the system, after which their total effect is measured to solve the MHE problem and determine the new set of estimates. This information is used to re-compute the optimal control setpoints at the next time instant, using updated information provided by the upper layer.

VIII. Simulation

A. Experimental design

The combination of different tidal periods (high and low tides), tidal ranges (spring, intermediate and neap tides), and navigational and non-navigational cycles gives rise to twelve different operating modes during system operation. Figure 6 presents the evolution of the previous aspects for a simulation horizon of one week, as well as the associated operating modes. It is recalled that the Calais canal is characterized by a semidiurnal tidal period, and thus transitions between high and low tides occur every six hours. Moreover, the simulation is set to begin towards the end of a neap tide so that system evolution throughout the three different tidal ranges can be simulated. Furthermore, navigational cycles for the Calais canal span from 6 a.m. to 8 p.m.

Each of the twelve operating modes may be described by a different objective prioritization. In practice, however, different tidal ranges only have an impact on the flows delivered by the gate, but do not introduce different prioritizations. Table III summarizes the choice of hierarchy of objectives introduced in Section V-A—including modifications discussed in Remark

This article has been accepted for publication in IEEE Transactions on Control Systems Technology. This is the author's version which has not been fully edited and content may change prior to final publication. Citation information: DOI 10.1109/TCST.2023.3309503

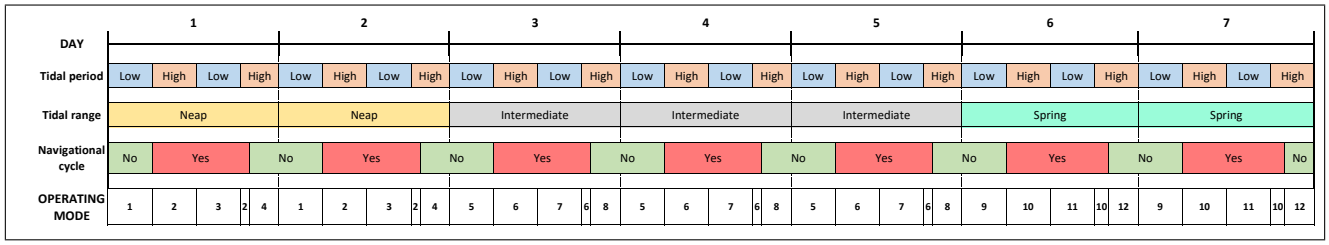

Fig. 6. Evolution of environmental and operational aspects, and associated operating modes

TABLE III
OBJECTIVE PRIORITIES FOR EACH OPERATING MODE

Objective	Operating mode			
	High tide, navigation	High tide, no navigation	Low tide, navigation	Low tide, no navigation
$J_k^{(1)}$	1	2	1	3
$J_k^{(2)}$	2	4	2	6
$J_k^{(3,g)}$	n/a	n/a	4	2
$J_k^{(3p)}$	3	1	3	1
$J_k^{(4,g)}$	n/a	n/a	6	5
$J_k^{(4,p)}$	4	3	5	4

3—for the combination of low/high tide and navigational/non-navigational cycles. Objectives are ranked according to the following guidelines:

- The first objective (maintain the levels within the navigation interval as much as possible) is deemed to be very relevant regardless of the operating mode.
- The second objective (setpoint tracking) is considered to be important only during navigational cycles, and minimal attention needs to be paid otherwise.
- Penalties on economic costs derived from the operation of the sea outlet gate and the pumps, which are reflected by means of $J_k^{(3,g)}$ and $J_k^{(3,p)}$, respectively, are considered to be the most important objectives during non-navigational periods. Moreover, pump usage minimization is deemed to be more important than that of the sea outlet gate. Note also that gate usage need not be optimized during high tide periods, as gates cannot be used.
- Smoothness of gate and pump control actions, expressed by means of $J_k^{(4,g)}$ and $J_k^{(4,p)}$, are generally considered to be the least important objectives. The only exception is setpoint tracking, which becomes the least important objective during non-navigational cycles. Again, $J_k^{(4,g)}$ need not be optimized during high tide periods.

Three disturbance profiles are generated using diverse combinations of the design flows provided in Figure 2. The scenarios, which are depicted in Figure 7, consider various disturbance intensities and frequencies as the result of different system conditions. Given the fact that access to the real system is not feasible, these disturbances are injected into a model of the system built using SIC^2 (Simulation and Integration of Control for Canals[1]). This hydraulic software package, which employs numerical methods to solve the Saint-Venant

[1]http://sic.g-eau.net

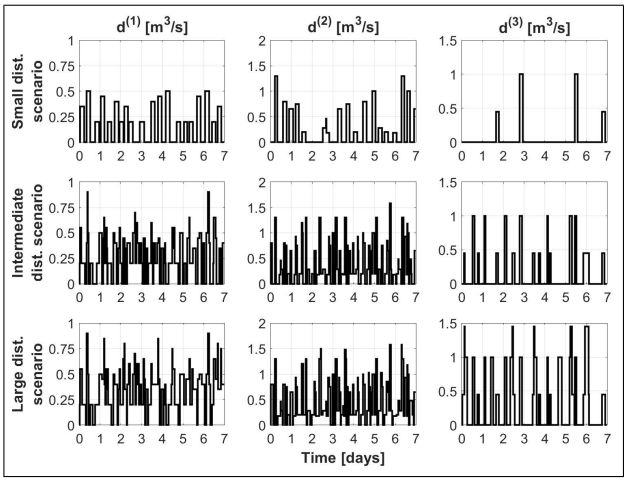

Fig. 7. Small, intermediate and large disturbance scenarios

equations, is widely used by hydraulic and control researchers to validate engineering solutions [53], [54], [55].

The following values of the design parameters are selected. Both the MPC prediction horizon H_p in (10) and the sliding window length N in (11) are set equal to thirty hours. Moreover, T_{s_1} and T_{s_2}, which correspond to the sampling times of the intermediate and lower layers, are chosen to be equal to 30 and 5 minutes, respectively. As water canals are characterized by slow dynamics, large sampling times may be selected. Furthermore, the amount of consecutive time instants during which the same low-level gate and pumping actions must be applied, i.e., l_g in (14c) and l_p in (17c), are set equal to two (ten minutes) and three (fifteen minutes), respectively. This is in line with real operation of the equipment, and reflects the fact that switching the activation state of a pump requires more time than operating a gate.

The evolution of the system is simulated in a computer with an Intel Core i7-8665U processor running at 1.9GHz with 8GB RAM. Moreover, results are obtained in Matlab R2020b using IBM ILOG CPLEX Optimization Studio V12.10.0 and the YALMIP toolbox [56].

B. Results

The three disturbance profiles depicted in Figure 7 are tested individually to assess system performance. A general analysis of the results for the ensemble of the scenarios is provided first. An in-depth analysis of one scenario is presented later.

1) General analysis of all scenarios: The accumulated values of the operational objectives described in Section V-A1

This article has been accepted for publication in IEEE Transactions on Control Systems Technology. This is the author's version which has not been fully edited and content may change prior to final publication. Citation information: DOI 10.1109/TCST.2023.3309503

over the complete one-week period are defined as $J^{(r)} \triangleq \sum_{i=0}^{t_{sim}} J_i^{(r)}$. These values are summarized in Table IV for all disturbance scenarios, and indicate that larger disturbances incur larger operational costs for the objectives.

Each operational objective defines a different performance metric, which are expressed using different units. Thus, a direct comparison of the values does not provide meaningful insight. However, $J^{(1)}$ and $J^{(2)}$ are both linked to the levels and are expressed in m^2, while $J^{(3,g)}$, $J^{(3,p)}$, $J^{(4,g)}$ and $J^{(4,p)}$ are linked to the control actions—the first two terms are expressed in economic units, and the last two, in $\mathrm{m}^6/\mathrm{s}^2$.

It can be observed that $J^{(1)} = 0$ for all scenarios, hence the control strategy succeeds in keeping the levels inside the navigation interval during the whole simulation. This behavior is aligned with the relative priorities provided in Table III, as compliance with the navigation interval is always among the most important objectives. On the other hand, $J^{(2)}$ exhibits larger values than $J^{(1)}$ for all scenarios, together with increasing values for increased disturbance magnitudes and frequencies. This behavior can be explained by the fact that $J^{(2)}$ becomes the least important objective during non-navigational cycles, which complicates its attainment.

With regard to the operational objectives linked to the control actions, $J^{(3,g)}$ exhibits lower values than the rest. While this behavior does not seem to align well with the relative priorities defined in Table III, it can be explained by the limitations in terms of gate usage. Gates can only be used during low-tide periods, a fact that requires to use pumps inevitably during high-tide periods, even if pump usage minimization is sought. However, the higher relative priority of $J^{(3,p)}$ can be observed in Table IV in that its values remain almost constant, regardless of the scenario. This allows to conclude that usage of pumps for the small disturbance scenario represents the bare minimum, and only minor additional pumpings are necessary for increased disturbances. On the other hand, the values of $J^{(4,g)}$ and $J^{(4,p)}$ are a consequence of the same explanations reported for $J^{(3,g)}$ and $J^{(3,p)}$.

2) Detailed analysis of a single disturbance scenario: For the sake of brevity, only the results corresponding to the large disturbance scenario are presented and discussed hereinafter.

The upper layer determines the current operating mode according to the system evolution depicted in Figure 6. This information is used to solve the corresponding MPC at the intermediate layer, yielding the optimal control setpoints depicted in Figure 8. It can be observed that the pumps are used more intensively than the gate, a behavior that could be regarded as undesirable given the priorities specified in Table III. However, this can be explained by the fact that the transition from non-navigational to navigational cycles coincides with the transition from low-tide to high-tide periods, as shown in Figure 6. The change in navigational cycle modifies the hierarchy of objectives (from reduced control effort to reduced level tracking error), while the tidal period transition only allows to use the pumps. Therefore, the larger effort in steering the levels back to the setpoints must be carried out by the pumps. Then, once a new low-tide period starts, only minimal effort is required from the gate to reject the disturbances and keep the levels close to the setpoints. On the other hand, the impossibility to use the gates during high tide is respected by the solution, as optimal gate setpoints are different from zero alternately, matching the low-tide periods.

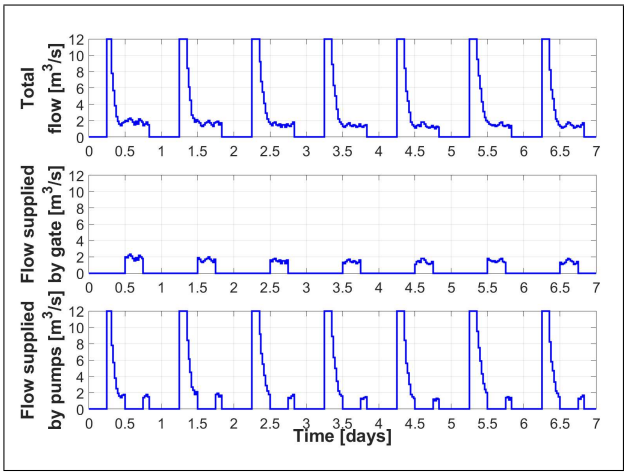

Fig. 8. Optimal setpoints

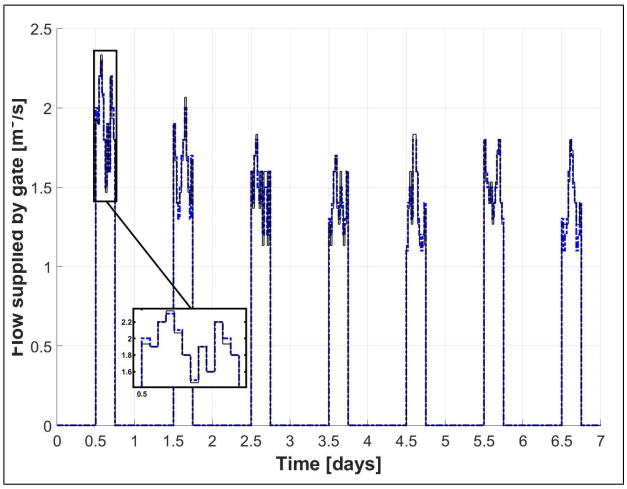

Fig. 9. Solution of the gate scheduling problem: optimal setpoints (blue solid) and low-level actions (black dashed)

The corresponding optimal setpoints depicted in Figure 8 are sent to the lower layer, and two scheduling problems are solved. Scheduling sequences for the gate and the pumps are determined and depicted in Figures 9 and 10, respectively. Non-smooth control signals are obtained, which is due to the low importance of $J_k^{(4)}$ on the one hand, and the combination of time scales and required water volumes on the other hand. Moreover, the mismatches between the intermediate and lower layer solutions are assessed by comparing the values of the operational objectives linked to the control signals. The results are summarized in Table V, and allow to conclude that the loss of performance resulting from applying the low-level actions instead of the optimal setpoints is minimal. Naturally, the degree of accuracy depends on the granularity of the discrete actuators—the coarser their resolution, the larger the expected mismatch is—and the choice of T_{s_1} and T_{s_2}. Furthermore, the sequential activation of the pumps imposed through (17e) can be realized in Figure 10.

Finally, the water level measurements that result from

This article has been accepted for publication in IEEE Transactions on Control Systems Technology. This is the author's version which has not been fully edited and content may change prior to final publication. Citation information: DOI 10.1109/TCST.2023.3309503

TABLE IV
ACCUMULATED COSTS OVER THE ENTIRE SIMULATION FOR DIFFERENT DISTURBANCE SCENARIOS

Disturbance magnitude and frequency	Operational objectives					
	$J^{(1)}\ (\mathrm{m}^2)$	$J^{(2)}\ (\mathrm{m}^2)$	$J^{(3,g)}$ (economic units)	$J^{(3,p)}$ (economic units)	$J^{(4,g)}\ (\mathrm{m}^6/\mathrm{s}^2)$	$J^{(4,p)}\ (\mathrm{m}^6/\mathrm{s}^2)$
Small	0	0.42	25.47	166.88	47.36	1150.77
Intermediate	0	0.68	31.06	169.33	57.92	1189.62
Large	0	0.90	38.98	171.87	66.25	1223.52

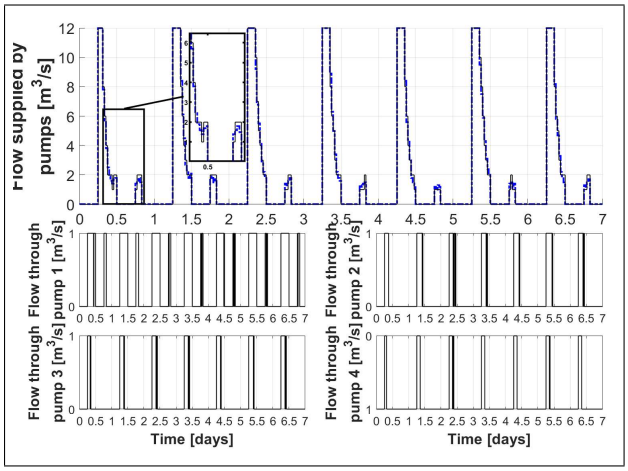

Fig. 10. Solution of the pumping scheduling problem: optimal setpoints (blue solid) and low-level actions (black dashed), and activation states

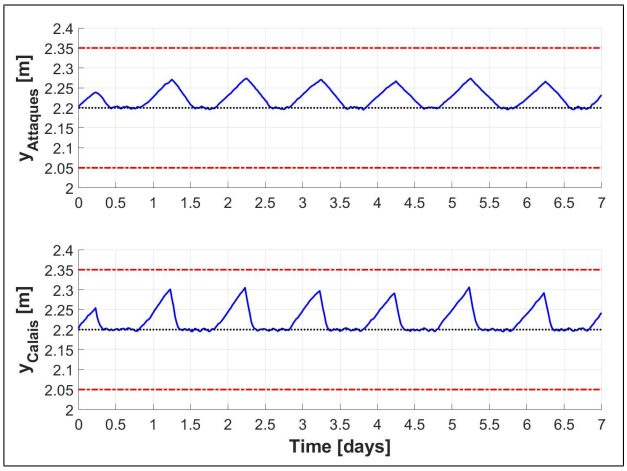

Fig. 11. Water levels (blue solid), NNL (black dotted), and LNL and HNL (red dashed)

TABLE V
PERFORMANCE COMPARISON BETWEEN INTERMEDIATE AND LOWER LAYER SOLUTIONS

Solution	Operational objectives			
	$J^{(3,g)}$	$J^{(3,p)}$	$J^{(4,g)}$	$J^{(4,p)}$
Intermediate layer (optimal)	38.98	171.87	66.25	1223.52
Lower layer (low-level)	39.26	176.75	66.48	1246.12
Relative loss of performance (%)	0.72	2.84	0.35	1.85

applying the low-level control actions are depicted in Figure 11. Two main aspects connected to water level regulation are expected to be achieved during system operation: compliance with the navigation interval and setpoint tracking. The former is always achieved, which can be realized by the fact that the water levels are never lower than the LNL or higher than the HNL. The latter becomes the least important objective during non-navigational cycles, and therefore levels are allowed to rise during these periods at the benefit of zero control effort as long as the water levels remain within bounds, which aligns well with the priorities defined in Table III. Nevertheless, the control strategy tries to steer the levels to the setpoints as soon as the next navigational cycle starts, leading to smooth water level fluctuations.

IX. CONCLUSIONS

This paper presented the design of a tailored control strategy for the Calais canal. This navigation canal is characterized by dynamics affected by tides, presence of discrete-valued actuators and a time-varying hierarchy of operational objectives. These features render a single-layer centralized implementation impractical, and a three-layer control architecture is proposed instead.

The upper layer determines the operating mode based on knowledge regarding environmental and operational aspects. Moreover, transitions between operating modes are assumed to be known. While this is true for navigational and non-navigational cycles, environmental phenomena such as tides are bound to be characterized by a small degree of uncertainty. Therefore, improvement of the current methodology could explore the formulation of mode commutations using a mixed logical dynamic representation, where a logic variable, e.g., comparison of sea and canal water levels, characterizes the overall system behavior.

The intermediate layer receives information regarding the current operating mode, and makes the corresponding adjustments to solve the appropriate MPC and MHE. A linear control-oriented model based on simplifications of the Saint-Venant equations is used to represent the system dynamics. This model is sufficiently accurate for the problem at hand, as the navigation interval within which the levels should be kept is rather narrow. However, the applicability of this modeling approach to other canals characterized by larger operating ranges could be compromised. To mitigate this issue, future work could regard the formulation of system dynamics in the linear-parameter varying framework using the results in [57].

MPC and MHE resolution is carried out by a single computing agent, an approach that can suffer from scalability issues and jeopardize reliability. The proposed approach could also be improved by making use of available results on distributed MPC [58] and robust distributed MHE [59]. Integration of these approaches within the multi-layer architecture presented in this work would allow to consider larger case studies, mitigate computational burden and incorporate robustness.

Furthermore, the disturbance estimation strategy used in the MPC scheme could be improved in several ways, for instance by assuming that the disturbance remains constant throughout the prediction horizon in the MPC, thus inducing an integrator in the model. Then, the model of the plant could be augmented with such a disturbance model, following the approach reported in [60].

The lexicographic approach is used to solve the problems, assuming that the decision maker can provide an a-priori list of preferences for the objectives. While this is realistic for few objectives such as in the current case study, establishing a clear ordered list could be challenging for a larger number of objectives. It could then be of interest to explore interactive or a-posteriori approaches to address more complex cases.

The lower layer receives the optimal control setpoints and solves two scheduling problems, one for the sea outlet gate and another for the pumps. As a result, feasible low-level actions are computed and applied to the system, upon which measurements can be taken and the process can be repeated at the next time instant. Nevertheless, the proposed approach assumes that neither sensors nor actuators are affected by faults, a situation that might arise in practice. Therefore, the inclusion of sensor and actuator fault mechanisms within the control loop could ensure satisfactory system performance even in the presence of faults.

ACKNOWLEDGMENT

The authors gratefully acknowledge the valuable feedback given by reviewers.

REFERENCES

[1] S. Mihic, M. Golusin, and M. Mihajlovic, "Policy and promotion of sustainable inland waterway transport in Europe–Danube River," *Renewable and sustainable energy reviews*, vol. 15, no. 4, pp. 1801–1809, 2011.

[2] Intergovernmental Panel on Climate Change, *Climate Change 2021: The Physical Science Basis. Contribution of Working Group I to the Sixth Assessment Report of the Intergovernmental Panel on Climate Change*. Cambridge University Press, 2021.

[3] A. Castelletti, A. Ficchì, A. Cominola, P. Segovia, M. Giuliani, W. Wu, S. Lucia, C. Ocampo-Martinez, B. De Schutter, and J. M. Maestre, "Model predictive control of water resources systems: A review and research agenda," *Annual Reviews in Control*, vol. 55, pp. 442–465, 2023.

[4] E. F. Camacho and C. Bordons, *Model Predictive Control*. London: Springer, 1998.

[5] J. B. Rawlings and D. Q. Mayne, *Model predictive control: theory and design*. Nob Hill Pub. Madison, Wisconsin, 2009.

[6] A. Zafra-Cabeza, J. M. Maestre, M. A. Ridao, E. F. Camacho, and L. Sánchez, "A hierarchical distributed model predictive control approach to irrigation canals: a risk mitigation perspective," *Journal of Process Control*, vol. 21, no. 5, pp. 787–799, 2011.

[7] S. M. Hashemy, M. J. Monem, J. M. Maestre, and P. J. van Overloop, "Application of an in-line storage strategy to improve the operational performance of main irrigation canals using model predictive control," *Journal of Irrigation and Drainage Engineering*, vol. 139, no. 8, pp. 635–644, 2013.

[8] F. Fele, J. M. Maestre, S. M. Hashemy, D. Muñoz de la Peña, and E. F. Camacho, "Coalitional model predictive control of an irrigation canal," *Journal of Process Control*, vol. 24, no. 4, pp. 314–325, 2014.

[9] D. Delgoda, H. Malano, S. K. Saleem, and M. N. Halgamuge, "Irrigation control based on model predictive control (MPC): Formulation of theory and validation using weather forecast data and AQUACROP model," *Environmental Modelling & Software*, vol. 78, pp. 40–53, 2016.

[10] A. Sadowska, P. J. van Overloop, C. Burt, and B. D. Schutter, "Hierarchical operation of water level controllers: Formal analysis and application on a large scale irrigation canal," *Water Resources Management*, vol. 28, no. 14, pp. 4999–5019, 2014.

[11] A. Sadowska, B. De Schutter, and P. J. van Overloop, "Delivery-oriented hierarchical predictive control of an irrigation canal: Event-driven versus time-driven approaches," *IEEE Transactions on Control Systems Technology*, vol. 23, no. 5, pp. 1701–1716, 2015.

[12] B. E. Aydin, X. Tian, J. Delsman, G. H. P. Oude Essink, M. Rutten, and E. Abraham, "Optimal salinity and water level control of water courses using model predictive control," *Environmental Modelling & Software*, vol. 112, pp. 36–45, 2019.

[13] H. A. Nasir, A. Carè, and E. Weyer, "A Scenario-Based Stochastic MPC Approach for Problems With Normal and Rare Operations With an Application to Rivers," *IEEE Transactions on Control Systems Technology*, vol. 27, no. 4, pp. 1397–1410, 2019.

[14] B. E. Aydin, G. H. P. O. Essink, J. R. Delsman, N. van de Giesen, and E. Abraham, "Nonlinear model predictive control of salinity and water level in polder networks: Case study of Lissertocht catchment," *Agricultural Water Management*, vol. 264, APR 30 2022.

[15] T. Ikeda, M. Nagahara, and S. Ono, "Discrete-valued control of linear time-invariant systems by sum-of-absolute-values optimization," *IEEE Transactions on Automatic Control*, vol. 62, no. 6, pp. 2750–2763, 2017.

[16] X. Tian, R. R. Negenborn, P. J. van Overloop, J. M. Maestre, A. Sadowska, and N. van de Giesen, "Efficient multi-scenario model predictive control for water resources management with ensemble streamflow forecasts," *Advances in Water Resources*, vol. 109, pp. 58–68, 2017.

[17] X. Tian, B. E. Aydin, R. R. Negenborn, N. van de Giesen, and J. M. Maestre, "Model predictive control for water level control in the case of spills," *Journal of Irrigation and Drainage Engineering*, vol. 143, no. 3, SI, 2017.

[18] P. Segovia, E. Duviella, and V. Puig, "Multi-layer model predictive control of inland waterways with continuous and discrete actuators," *IFAC-PapersOnLine*, vol. 53, no. 2, pp. 16 624–16 629, 2020, 21st IFAC World Congress.

[19] F. K. Pour, P. Segovia, E. Duviella, and V. Puig, "A two-layer control architecture for operational management and hydroelectricity production maximization in inland waterways using model predictive control," *Control Engineering Practice*, vol. 124, JUL 2022.

[20] K. Horvath, B. van Esch, T. Vreeken, T. Piovesan, J. Talsma, and I. Pothof, "Potential of model predictive control of a polder water system including pumps, weirs and gates," *Journal of Process Control*, vol. 119, pp. 128–140, 2022.

[21] X. Tian, Y. Guo, R. R. Negenborn, L. Wei, N. M. Lin, and J. M. Maestre, "Multi-scenario model predictive control based on genetic algorithms for level regulation of open water systems under ensemble forecasts," *Water Resources Management*, vol. 33, no. 9, pp. 3025–3040, 2019.

[22] P. Velarde, X. Tian, A. Sadowska, and J. M. Maestre, "Scenario-Based Hierarchical and Distributed MPC for Water Resources Management with Dynamical Uncertainty," *Water Resources Management*, vol. 33, no. 2, pp. 677–696, 2019.

[23] P. Tatjewski, "Advanced control and on-line process optimization in multilayer structures," *Annual Reviews in Control*, vol. 32, no. 1, pp. 71–85, 2008.

[24] Z. Dong, Z. Zhang, Y. Dong, and X. Huang, "Multi-layer perception based model predictive control for the thermal power of nuclear superheated-steam supply systems," *Energy*, vol. 151, pp. 116–125, 2018.

[25] A. Ibrahim, D. Goswami, H. Li, I. M. Soroa, and T. Basten, "Multi-layer multi-rate model predictive control for vehicle platooning under IEEE 802.11p," *Transportation Research Part C: Emerging Technologies*, vol. 124, p. 102905, 2021.

[26] D. T. Machacek, K. Barhoumi, J. M. Ritzmann, T. Huber, and C. H. Onder, "Multi-level model predictive control for the energy management of hybrid electric vehicles including thermal derating," *IEEE Transactions on Vehicular Technology*, vol. 71, no. 10, pp. 10 400–10 414, 2022.

[27] P. Guekam, P. Segovia, L. Etienne, and E. Duviella, "Hierarchical model predictive control and moving horizon estimation for open-channel systems with multiple time delays," in *2021 European Control Conference (ECC)*, 2021, pp. 198–203.

[28] M. Cantoni, E. Weyer, Y. Li, S. K. Ooi, I. Mareels, and M. Ryan, "Control of large-scale irrigation networks," *Proceedings of the IEEE*, vol. 95, no. 1, pp. 75–91, 2007.

[29] E. Weyer, "Control of irrigation channels," *IEEE Transactions on Control Systems Technology*, vol. 16, no. 4, pp. 664–675, 2008.

[30] M. Foo, S. K. Ooi, and E. Weyer, "System identification and control of the broken river," *IEEE Transactions on Control Systems Technology*, vol. 22, no. 2, pp. 618–634, 2014.

[31] H. A. Nasir, M. Cantoni, Y. Li, and E. Weyer, "Stochastic model predictive control based reference planning for automated open-water channels," *IEEE Transactions on Control Systems Technology*, vol. 29, no. 2, pp. 607–619, 2021.

[32] C. Ocampo-Martinez, A. Ingimundarson, V. Puig, and J. Quevedo, "Objective Prioritization Using Lexicographic Minimizers for MPC of Sewer Networks," *IEEE Transactions on Control Systems Technology*, vol. 16, no. 1, pp. 113–121, 2008.

[33] J. Wagenpfeil, E. Arnold, H. Linke, and O. Sawodny, "Modelling and optimized water management of artificial inland waterway systems," *Journal of Hydroinformatics*, vol. 15, no. 2, pp. 348–365, 2012.

[34] J. Galindo, S. Torok, F. Salguero, S. de Campos, J. Romera, and V. Puig, "Optimal Management of Water and Energy in Irrigation Systems: Application to the Bardenas Canal," *IFAC-PapersOnLine*, vol. 50, no. 1, pp. 6613–6618, 2017, 20th IFAC World Congress.

[35] E. Duviella and B. Hadid, "Simulation tool of the Calais Canal implementing Logic Control based regulation," *IFAC-PapersOnLine*, vol. 52, no. 23, pp. 23–28, 2019.

[36] X. Litrico and V. Fromion, "Simplified modeling of irrigation canals for controller design," *Journal of Irrigation and Drainage Engineering*, vol. 130, no. 5, pp. 373–383, 2004.

[37] ——, *Modeling and Control of Hydrosystems*. Springer, 2009.

[38] P. Segovia, L. Rajaoarisoa, F. Nejjari, E. Duviella, and V. Puig, "Model predictive control and moving horizon estimation for water level regulation in inland waterways," *Journal of Process Control*, vol. 76, pp. 1–14, 2019.

[39] P. J. Antsaklis and A. N. Michel, *A linear systems primer*. Springer Science & Business Media, 2007.

[40] D. Q. Mayne, J. B. Rawlings, C. V. Rao, and P. O. M. Scokaert, "Constrained model predictive control: Stability and optimality," *Automatica*, vol. 36, no. 6, pp. 789–814, 2000.

[41] D. Pugh and P. Woodworth, *Sea-level science: understanding tides, surges, tsunamis and mean sea-level changes*. Cambridge University Press, 2014.

[42] "National Oceanic and Atmospheric Administration," https://oceanservice.noaa.gov/education/tutorial_tides/tides07_cycles.html, accessed: 2021-11-30.

[43] S. Plaschke, M. Bulla, M. Cruz-López, S. G. del Ángel, and C. Küpper, "Nest initiation and flooding in response to season and semi-lunar spring tides in a ground-nesting shorebird," *Frontiers in Zoology*, vol. 16, no. 1, 2019.

[44] M. L. Tyler and M. Morari, "Propositional logic in control and monitoring problems," *Automatica*, vol. 35, no. 4, pp. 565–582, Apr. 1999.

[45] J. B. Rawlings and B. T. Stewart, "Coordinating multiple optimization-based controllers: New opportunities and challenges," *Journal of Process Control*, vol. 18, no. 9, pp. 839 – 845, 2008.

[46] A. Castelletti and R. Soncini-Sessa, "A procedural approach to strengthening integration and participation in water resource planning," *Environmental Modelling & Software*, vol. 21, no. 10, pp. 1455–1470, 2006.

[47] A. Castelletti, A. V. Lotov, and R. Soncini-Sessa, "Visualization-based multi-objective improvement of environmental decision-making using linearization of response surfaces," *Environmental Modelling & Software*, vol. 25, no. 12, pp. 1552–1564, 2010.

[48] E. C. Kerrigan and J. M. Maciejowski, "Designing model predictive controllers with prioritised constraints and objectives," in *Proceedings. IEEE International Symposium on Computer Aided Control System Design*, 2002, pp. 33–38.

[49] C. V. Rao, "Moving horizon strategies for the constrained monitoring and control of nonlinear discrete-time systems," Ph.D. dissertation, University of Wisconsin–Madison, 2000.

[50] D. Copp and J. Hespanha, "Simultaneous nonlinear model predictive control and state estimation," *Automatica*, vol. 77, pp. 143–154, 2017.

[51] C. V. Rao, J. B. Rawlings, and J. H. Lee, "Constrained linear state estimation – a moving horizon approach," *Automatica*, vol. 37, no. 10, pp. 1619–1628, 2001.

[52] D. Bertsimas, E. Litvinov, X. Sun, J. Zhao, and T. Zheng, "Adaptive robust optimization for the security constrained unit commitment problem," *IEEE Transactions on Power Systems*, vol. 28, no. 1, pp. 52–63, 2013.

[53] K. Horváth, E. Galvis, M. Gómez, and J. Rodellar, "New offset-free method for model predictive control of open channels," *Control Engineering Practice*, vol. 41, pp. 13–25, 2015.

[54] H. Oubanas, I. Gejadze, P. O. Malaterre, and F. Mercier, "River discharge estimation from synthetic SWOT-type observations using variational data assimilation and the full Saint-Venant hydraulic model," *Journal of Hydrology*, vol. 559, pp. 638–647, 2018.

[55] M. Luppi, P. O. Malaterre, A. Battilani, V. Di Federico, and A. Toscano, "A Multi-disciplinary Modelling Approach for Discharge Reconstruction in Irrigation Canals: The Canale Emiliano Romagnolo (Northern Italy) Case Study," *Water*, vol. 10, no. 8, 2018.

[56] J. Löfberg, "YALMIP: a toolbox for modeling and optimization in MATLAB," in *IEEE International Symposium on Computer Aided Control Systems Design*, Taipei, Taiwan, 2004.

[57] Y. Bolea, V. Puig, and J. Blesa, "Linear parameter varying modeling and identification for real-time control of open-flow irrigation canals," *Environmental Modelling & Software*, vol. 53, pp. 87–97, 2014.

[58] P. Segovia, V. Puig, E. Duviella, and L. Etienne, "Distributed model predictive control using optimality condition decomposition and community detection," *Journal of Process Control*, vol. 99, pp. 54–68, 2021.

[59] P. Segovia, V. Puig, and E. Duviella, "Set-membership-based distributed moving horizon estimation of large-scale systems," *ISA Transactions*, 2021.

[60] G. Pannocchia and J. Rawlings, "Disturbance models for offset-free model-predictive control," *AIChE Journal*, vol. 49, no. 2, pp. 426–437, 2003.

Pablo Segovia received his BS/MS degree in Industrial Engineering in 2015 from Universitat Politècnica de Catalunya (UPC), Barcelona, Spain, and his Ph.D. degree in Automatic control, Robotics and Vision in 2019 from UPC and IMT Lille Douai, Lille, France. He has held postdoctoral research appointments at IMT Lille Douai (2019–2020), Delft University of Technology, the Netherlands (2020–2023) and UPC (2023–present). His research interests include large-scale systems management using non-centralized predictive control approaches, with applications to water resources systems and intelligent transportation systems.

Vicenç Puig received his BS/MS degree in telecommunications engineering in 1993 and his PhD degree in Automatic Control, Robotics and Computer Vision in 1999, both from the Universitat Politècnica de Catalunya (UPC), Barcelona, Spain. He is a full professor at the Automatic Control Department of UPC and a researcher at the Institute of Robotics and Industrial Informatics (IRI), CSIC–UPC. He is the director of the Automatic Control Department and the head of the Research Group on Advanced Control Systems (SAC) at UPC. He has made important scientific contributions in the areas of fault diagnosis and fault tolerant control, using interval and linear-parameter-varying models exploiting set-based approaches. He is currently the chair of the IFAC Safeprocess TC Committee 6.4. He was the general chair of the 3rd IEEE Conference on Control and Fault-Tolerant Systems (SysTol 2016) and the IPC chair of IFAC Safeprocess 2018.

Eric Duviella received a "diplôme d'ingénieur" from Ecole Nationale d'Ingénieurs de Tarbes (ENIT) and an M.S. from Institut National Polytechnique de Toulouse (INPT), both in 2001. In 2005, he obtained a Ph.D. degree in Industrial Systems from Institut National Polytechnique de Toulouse. From September 2004 to August 2006, he worked at Ecole Nationale d'Ingénieurs de Tarbes as temporary assistant professor (ATER). In September 2006, he achieved a postdoctoral position in the Laboratoire d'Automatique, Génie Informatique et Signal (Lagis) in Lille. Since January 2007, he has held a permanent position of assistant professor in the department of Automatic Control and Computer Sciences at Ecole des Mines de Douai, France. In 2014, he obtained an HDR ("Habilité à Diriger des Recherches"). Since November 2015, he is Professor of the Institut Mines Telecom Nord Europe